Dynamics of the Triplet State of a Dithiophene in Different Solid Matrixes Studied by Transient and Pulse EPR Techniques

Antonio Barbon,[†] Marco Bortolus,[†] Marina Brustolon,*[,†] Angiolina Comotti,[‡] Anna Lisa Maniero,[†] Ulderico Segre,[§] and Piero Sozzani[‡]

Dipartimento di Chimica Fisica, Università di Padova, Via Loredan 2, 35131 Padova, Italy, Dipartimento di Scienza dei Materiali, Università di Milano-Bicocca, Via Cozzi 53, 20125 Milano, Italy, and Dipartimento di Chimica, Università di Modena e Reggio Emilia, Via Campi 183, 41100 Modena, Italy

Received: May 31, 2002; In Final Form: January 17, 2003

The photoexcited triplet state of a 4-4′-disubstituted dithiophene has been investigated by time-resolved electron paramagnetic resonance in two different solid matrixes—glassy toluene which acts as an amorphous isotropic medium and a spirocyclophosphazene inclusion compound—which provides an ordered confining structure to the guest molecules. Different spectral line shapes with different temperature dependence have been obtained using continuous-wave or spin−echo detection. This behavior was attributed to spin relaxation due to modulation of the zero-field splitting tensor induced by fast librational motion of the dithiophene triplet. Moreover, differences between line shapes in the two matrixes were reproduced considering a librational motion occurring preferentially around different molecular axes.

Introduction

The physicochemical and spectroscopic properties of single molecules when dispersed in a medium and isolated one from the other can be modulated by the environment.[1] The modulation becomes fine-tuned if an organized medium is adopted and the matrix is structured in such a way to host the molecules in nanoscale cavities of uniform size and dimension.

Excited and reactive states can be observed as confined in such a well-defined environment. In fact, there is considerable interest in the study of the singlet and triplet excited states of a vast class of polyconjugated molecules with nonlinear optical properties, such as second-harmonic generation (SHG) photoluminescence.[2−11] When confined, such molecules are described as producing materials substantially different from those in the bulk phases.[12−20] The supramolecular organization of the molecules follows novel assembly principles and topological constrains resulting in anisotropic alignments and different conformational and motional behaviors. This confinement produces a conformational constraint strongly analogous to natural host−guest systems formed by light acceptors and proteins in biological systems.

In the present paper we report an EPR study of the conformational and dynamical behavior of the photoexcited triplet state of a 4-4′-dipentoxy-2,2′-dithiophene (DT) molecule. The DT molecules were studied in the inclusion compound obtained with a spirocyclophosphazene (tris(*o*-phenylenedioxy) spirocyclotriphosfazene, TPP) as a host matrix. The host molecules self-assemble forming a crystalline architecture that provides parallel hexagonal channels available for the guest molecules.[21−24] For comparison we used a glassy toluene solution, as a model for an amorphous isotropic medium.

The detection of photoexcited triplet state can be a challenge for the researchers for the dilution and the short lifetime of the species. Our aim was achieved by time-resolved cw (TR-EPR) and echo-detected EPR (EchoEPR) spectroscopies. The spin polarization generated at the birth of the triplet state favors detection of species even at low stationary concentrations. The analysis of the TR-EPR spectra gives, beyond the magnitude of the fine interaction, the spin polarization originated from the spin selective population of the triplet sublevels at zero field. However, the profiles of the cw spectra depend mainly on the static inhomogeneous line width and are not sensitive to the motional processes.[25] Electron spin−echo techniques, in particular EchoEPR, provide a much more sensitive method with respect to cw EPR spectroscopy to monitor dynamical processes since pulsed experiments probe directly the homogeneous contribution to the line width which is due to the dynamical relaxation processes. The analysis of the spectra recorded at different temperatures allows to obtain information on the triplet state anisotropic molecular motion and to study the dependence of anisotropy on the organization of the media.

EchoEPR spectra are obtained by recording the electron spin−echo intensity as a function of the magnetic field at a fixed delay time τ between the two echo-forming pulses. The spectral profile of the EchoEPR spectra is therefore in general different from the corresponding cw EPR spectra depending on the differences between the phase memory times T_M of the spin packets on varying the magnetic field. For example, for spin probes in disordered matrixes, as polycrystalline powders or glassy phases, different relaxation rates at different field positions derive from a time modulation of anisotropic spin interactions as hyperfine or **g**-tensor interactions, due to residual motions.[26−28] In the case of the photoexcited triplet state of free-base porphycene, investigated by TR-EPR and EchoEPR techniques,[29] the dynamical modulation of the zero-field splitting (ZFS) interaction acted as an efficient anisotropic spin−spin relaxation mechanism. In that paper it was pointed out the complementary nature of the two acquisition techniques, and it

* To whom correspondence should be addressed. E-mail: m.brustolon@chfi.unipd.it.
[†] Dipartimento di Chimica Fisica.
[‡] Dipartimento di Scienza dei Materiali.
[§] Dipartimento di Chimica.

10.1021/jp026214f CCC: $25.00
Published on Web 03/18/2003

was suggested that anisotropic molecular motions in photoexcited triplet states may be investigated in much the same way, as it has been in doublet states in glassy phases.

Experimental Section

A Bruker ESP380E spectrometer with a dielectric resonator was used both for Time-Resolved cw EPR (TR-EPR) and for pulse experiments.

For TR-EPR measurements, a high-quality factor Q of the cavity and a corresponding slow detection line were used. In this experiment the signal, generated under continuous microwave irradiation, was taken from the detector, preamplified and digitalized from a LeCroy 3560 digital oscilloscope. The response time of the apparatus was estimated to be around 800 ns. A surface was obtained by acquiring the time decay traces for different field positions. Integration with time windows of around 400 ns allowed the obtaining of slices along the field.

For pulse experiments, an echo sequence $\pi/2$-τ-π-τ-echo was used after a time T of few tens of nanoseconds from the laser flash. The integrated echo intensity was recorded for different field positions (EchoEPR technique).

The optical irradiation was performed by laser flashes of 5 ns width at 355 nm produced by a Nd:YAG laser equipped with second- and third-harmonic generators. The light was conveyed into the cavity through an optical window in the cryostat; the cryostat (Oxford CF935) could use either liquid helium or nitrogen.

The solid samples or the solutions in toluene were degassed and sealed under vacuum.

The TPP inclusion compound (IC) with the dipentoxy-substituted bithienyl was obtained by crystallization from *o*-xylene solvent. The synthesis of tris(*o*-phenylenedioxy)-spirocyclotriphosfazene (TPP) and of 4-4′-dipentoxy-2,2′-dithiophene (DT) have been described elsewhere.[30,31] The *o*-xylene solvent (Fluka >99%) was further purified by *n*-nonane impurities using molecular sieves and the TPP matrix as entrapment agents of linear alkanes. The TPP IC has been characterized by calorimetric analysis, X-ray diffraction and ^{13}C solid-state NMR. The calorimetric trace of the IC shows a congruent melting at 296 °C, the melting point of the IC is higher than the melting of both TPP matrix and the pure bithienyl. The powder X-ray diffraction pattern indicates the formation of an hexagonal unit cell.[30] ^{13}C CPMAS NMR spectrum shows three main peaks in the aromatic region corresponding to the three carbons of the TPP matrix, each of them gives rise to a single resonance because of the equivalence of the same atoms in the hexagonal unit cell. All the resonances of the DT molecules show a downfield shift due to the magnetic susceptibility of the TPP molecules: these data demonstrate the formation of the adduct.

Results

We have obtained TR-EPR and EchoEPR spectra of the photogenerated triplet state of DT in glassy toluene matrix and in TPP inclusion matrix at 4 and 80 K to study the dynamics of the triplet state of DT in the two different matrixes.

We have measured T_M for the probe in toluene at $T = 4$ K for different values of the magnetic field along the spectrum. The values obtained are reported in Figure 1. One can clearly appreciate longer T_M's in correspondence of the principal values of the ZFS.

The phase memory times have been measured also for the two matrixes at 80 K for the field corresponding to the low-field Y component. Values of $T_M = 250$ ns and $T_M = 800$ ns have been obtained respectively for the probe in toluene and in TPP.

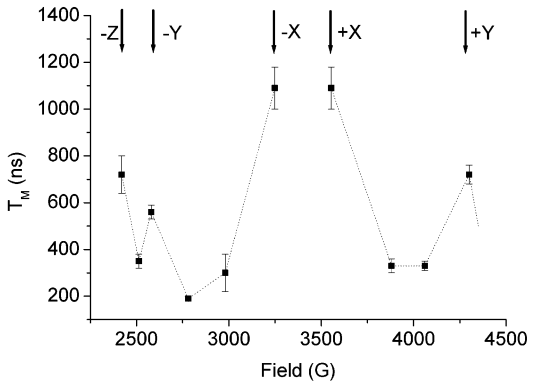

Figure 1. Phase memory time T_M of the photoexcited triplet of DT in toluene at 4 K for different field positions. The resonance positions relative to the principal values of the ZFS tensor are indicated by arrows. The echo decay curves were fitted with a linear exponential. The decay at the field position corresponding to the $+Z$ component was not obtained due to the low spectral intensity.

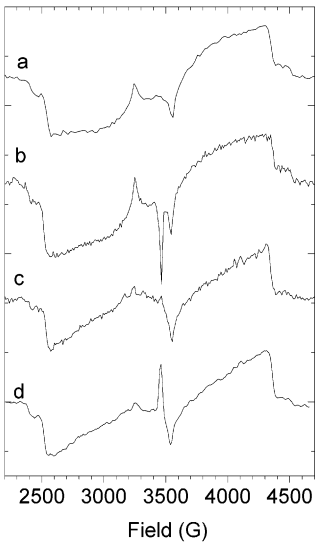

Figure 2. Spectra at 4 K of DT excited at 355 nm. (a) TR-EPR of DT in toluene glassy matrix at 1.5 μs after the laser flash. (b) TR-EPR of DT in the TPP inclusion compound at 1.5 μs after the laser flash; the narrow emissive line at $g = 2$ is attributed to polarized photoproduced radicals. (c) EchoEPR of DT in toluene glassy matrix obtained with a 16−160−32 ns echo sequence 50 ns after the laser flash. (d) EchoEPR of DT in TPP inclusion compound obtained with a 16−160−32 ns echo sequence ca. 50 ns after the laser flash; the narrow line at $g = 2$ is attributed to photoproduced radicals.

TR-EPR Spectra at 4 K. The TR-EPR at 4 K spectrum of DT in frozen toluene is ca. 2100 G wide (Figure 2a). The microwave (mw) low-power spectrum was taken ca. 1.5 μs after the laser flash, corresponding to the maximum of the signal intensity. The time dependence of the spectral profile shows after 5 μs a significant modification in intensity and in the line shape. On the other hand, identical spectral profiles with respect to the spectrum at 1.5 μs are obtained at earlier times. This allows a safe comparison with the EchoEPR spectra, see below.

The spectrum shows an EEA/EAA polarization pattern, due to the selective population of the ZFS levels with the state $|Y\rangle$ as the most populated.

The spectrum of DT in TPP inclusion compound recorded in the same conditions (Figure 2b) is similar to the previous

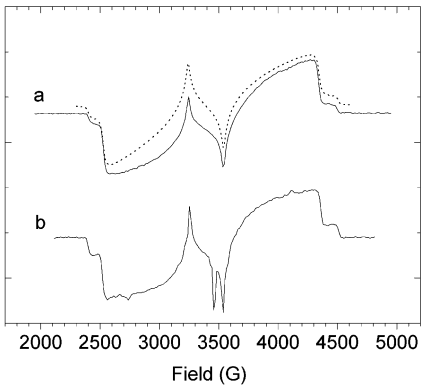

Figure 3. TR-EPR spectra at 80 K of DT excited at 355 nm. The spectra were recorded 1.5 μs after the laser flash. (a) toluene glassy matrix (dotted line for the simulation). Simulation parameters: ZFS parameters $D = 0.098$ cm^{-1} and $E = 0.023$ cm^{-1}; population of the triplet sublevels $(p_x-p_y):(p_x-p_z) = -0.77:-0.23$; g principal values are 2.009, 2.005, and 2.003. (b) TPP inclusion compound. The narrow emissive line at $g = 2$ is attributed to a polarized photoproduced radical.

one apart for the narrower line width of the *X* components and for the presence of an emissive narrow band around $g = 2$ attributed to polarized photoproduced radicals; these species have been observed also in other substituted oligothiophenes.[32]

EchoEPR Spectra at 4 K. The EchoEPR spectra recorded in the two matrixes ca. 50 ns after the laser flash are shown in Figure 2c,d.

We used a 16 ns $\pi/2$ pulse and a delay between pulses of $\tau = 160$ ns. With these parameters we obtained a reasonable signal-to-noise ratio at 4 K and at 80 K. Longer pulses gave spectra with a much worse signal-to-noise ratio. A drawback of the relatively short mw pulses, and therefore of the relatively large bandwidth, was the ESEEM modulation, particularly evident at the low-field values. The modulation was shallow or non existent for longer pulses. A comparison between the EchoEPR spectra at different pulse lengths was the guideline for finding the best τ value in order to minimize the distortion of the spectra due to nuclear modulation. In any case the modulation effect was found to be negligible at field values higher than that corresponding to the $+X$ component. Therefore we compared preferentially the high-field part of the spectra to the simulated ones, disregarding eventual inconsistencies at lower field values.

The EchoEPR spectra are similar to the corresponding TR-EPR spectra; in particular, they exhibit the same ZFS values and the same polarization pattern (EEA/EAA). They show an absorptive narrow band around $g = 2$ attributed to accumulated photoproduced radicals as found in analogous systems.[32] Apart from this signal, the main differences between the TR-EPR and EchoEPR spectra reside on the relative intensities of the spectral features at the different field values. In particular in the EchoEPR spectra the spectral intensities in correspondence to the principal directions of the ZFS tensor are larger than those at intermediate field values if compared with the respective intensities in the TR-EPR spectra.

TR-EPR Spectra at 80 K. At 80 K the TR-EPR spectrum in glassy toluene (Figure 3a) does not show dramatic changes with respect to the spectrum obtained at the lower temperature (Figure 2a). The differences are mainly due to a higher intensity of the *X* components, which reduce the extra structure observed at the lower temperature between these two components. No changes of the ZFS terms have been observed, within the experimental errors.

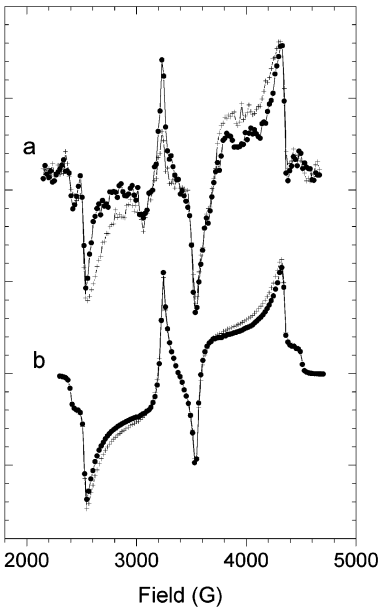

Figure 4. (a) Experimental EchoEPR at 80 K of DT in toluene glassy matrix for a delay time $\tau = 160$ ns (crosses) and $\tau = 200$ ns (circles). The spectra are normalized to evidence the shape modification with time. (b) Simulations of the normalized experimental EchoEPR spectra for a delay time $\tau = 160$ ns (crosses) and $\tau = 200$ ns (circles). The simulations were obtained with the parameters given in Figure 3. For the decay of the magnetization we used $(1/T_2)^0_X = 1000$ ns, $(1/T_2)^0_Y = 500$ ns, and $(1/T_2)^0_Z = 500$ ns and assumed a libration about the *Z* axis of the ZFS tensor with $\tau_L\varphi^2 = 1.7$ ps rad^2 (see text).

Also in the TPP matrix, the TR-EPR spectra at 4 and 80 K are very similar (see Figures 2b and 3b, respectively).

EchoEPR Spectra at 80 K. The EchoEPR spectra at 80 K in the two matrixes (Figures 4 and 5) are different from those at 4 K (Figure 2c,d). Moreover, they are substantially different from the TR-EPR spectra at the same temperature (Figure 3a,b). Evident differences are also present between the EchoEPR spectra in the two matrixes.

To put in perspective the different spectral features, we report the EchoEPR spectra in the two matrixes corresponding to two different delay times ($\tau = 160$ ns and $\tau = 200$ ns for the toluene matrix, and $\tau = 160$ ns and 320 ns for the TPP matrix).

As can be observed in Figure 4, in the toluene matrix the intensity of the EchoEPR spectrum between the *Y* and *X* components is strongly reduced, leading to a low-lying plateau with sharp edges in the vicinity of the *X* components. Also the spectra in the TPP matrix at 80 K (Figure 5) show an anisotropic decay of the magnetization at field positions between the *Y* and the *X* components, but they are more similar to those obtained at 4 K. As discussed later, the differences of the spectral profiles can be explained by considering an intermolecular motion of the probe, whose anisotropy depends on the matrix.

To summarize the results, we have found that, for both temperatures and matrixes, EchoEPR spectra have a modified spectral profile with respect to the corresponding TR-EPR spectra, due to a different decay of the magnetization along the principal directions of the ZFS tensor with respect to the other directions. Besides this, the spectral profiles are different in the two matrixes.

Simulations and Discussion

To simulate the low-power TR-EPR spectra, we used standard procedures for polarized triplet states produced via ISC.[33] For

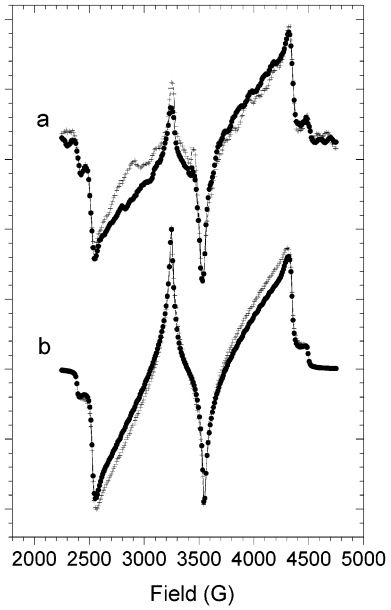

Figure 5. (a) Experimental EchoEPR at 80 K of DT in TPP inclusion compound for a delay time $\tau = 160$ ns (crosses) and $\tau = 320$ ns (circles); the narrow emissive line at $g = 2$ is attributed to photoproduced radicals. The spectra are normalized to put in evidence the shape modification with time. (b) Simulations of the normalized experimental EchoEPR spectra for $\tau = 160$ ns (crosses) and for $\tau = 320$ ns (circles). The simulations were obtained with the parameters given in Figure 3. For the decay of the magnetization we used $(1/T_M)^0_X = 1000$ ns, $(1/T_M)^0_Y = 1000$ ns, and $(1/T_M)^0_Z = 1000$ ns and assumed a libration about the Z axis of the ZFS tensor with $\tau_L\varphi^2 = 5.0$ ps rad^2 (see text).

the Hamiltonian we considered only the Zeeman and the fine term:[25]

$$H = \mu_B \mathbf{S}\cdot\mathbf{g}\cdot\mathbf{B} + \mathbf{S}\cdot\mathbf{D}\cdot\mathbf{S} \qquad (1)$$

The zero-field splitting (ZFS) tensor **D** is traceless, and its diagonal elements can be given as usually in terms of the parameters $D = (3/2)D_{zz}$ and $E = (1/2)(D_{xx} - D_{yy})$. The spectrum is calculated as a sum over all possible orientations of the magnetic field **B** in the ZFS reference system. We consider the fine term as a perturbation and the eigenvalues of the Hamiltonian are computed up to the second order (see Appendix). Each orientation, defined by a set of angles Ω, is characterized by two values of the resonant fields $B_{res}(\Omega)$, relative to the transition between the eigenstates $|-1\rangle \rightarrow |0\rangle$ (B_{res-}) and $|0\rangle \rightarrow |+1\rangle$ (B_{res+}). The relative intensity of any transition in the triplet manifold is proportional to the nonequilibrium population difference $P_{\pm}(\Omega)$ dependent on the mechanism of the excited triplet state generation. For triplet states populated by ISC, the populations are a linear combination of the zero-field states populations p_x, p_y, and p_z.[33] Then the total spectrum is calculated as

$$I(B) = \sum_{\pm} \int G(B_{res\pm}(\Omega) - B) P_{\pm}(\Omega)\, d\Omega \qquad (2)$$

where $G(x)$ is a line shape function. The second-order approximation allows us to reproduce correctly the positions of the spectral features, as reported in Figure 3, dotted line. The values of the parameters obtained from the best fitting simulations are $D = 0.098$ cm^{-1}, $E = 0.023$ cm^{-1}, $(p_x - p_y):(p_x - p_z) = -0.77:-0.23$, $g_x = 2.009$, $g_y = 2.005$, and $g_z = 2.003$.

To simulate the EchoEPR spectra, we have to take into account the different echo decay rates for the different spin packets. The experimental spectral intensity is lower in the regions between the fields corresponding to the ZFS principal values. This fact can be explained assuming a relaxation mechanism that produces a slower dephasing of the echo for those molecules with the principal directions of the ZFS oriented along the magnetic field.

As reported in the Introduction, a reorientational motion of the molecule in the magnetic field leads to modulation of orientationally dependent magnetic interactions as the hyperfine interaction, the effective g value, and the ZFS interactions. The modulation of the latter interaction is expected to be responsible of the dominating relaxation mechanism in the case of a triplet state with large ZFS values. The amplitude of the modulation of the resonance frequency $\Delta\omega$, for a motion around a given axis, will depend on the angular variation of the fine interaction for that particular rotation. The $\Delta\omega$ minima and therefore the slowest echo dephasing rates are expected to occur, as observed, for those molecules oriented with the ZFS principal directions along the magnetic field, corresponding to minima and maxima of the fine interaction. In this hypothesis the differences of the spectral profiles of EchoEPR spectra in toluene glass and in TPP at 80 K can be attributed to different anisotropies of the angular motions in the two matrixes.

On the basis of this model, the rate of the phase memory loss of the probe is supposed to be given for any orientation Ω by two different contributions, one $(1/T^m_M(\Omega,\Phi))$ due to the mechanism described above, and the other one $(1/T^0_M(\Omega))$ to any other relaxation process (as instantaneous diffusion, spectral diffusion, and nuclear spin flip-flops):[34,35]

$$\frac{1}{T_M(\Omega,\Phi)} = \frac{1}{T^0_M(\Omega)} + \frac{1}{T^m_M(\Omega,\Phi)} \qquad (3)$$

The phase memory time $T^m_M(\Omega,\Phi)$ characterizes the fast small-angle libration. We used a simplified model where the motion in a harmonic potential is considered as an exchange between two orientations with different resonance frequencies, the difference being $\Delta\omega(\Omega,\Phi)$. The two orientations are defined by a rotation of the molecule of an angle φ around an axis d. The librational angle should be very small from the evidence that the ZFS principal values do not change in the range 4−80 K. We will discuss further this point below.

The displacement of the director of the magnetic field is indicated by Φ. This process is dominating the relaxation, apart when the magnetic field is along the ZFS principal axes, where only the term $1/T^0_M(\Omega)$ in eq 3 is different from zero. To simulate correctly the EchoEPR intensities along the principal axes, for the toluene matrix this term was considered slightly dependent on the orientation. The echo decays measured at 4 K (Figure 1) show differences in the phase memory times in correspondence to the principal values of the ZFS similar to those used in the simulation.

By assuming for the exchange a correlation time τ_L, and the fast motion condition $\Delta\omega^2\tau_L^2 \ll 1$, the contribution of the libration motion to the phase memory time can be written as[36]

$$T^m_M(\Omega,\Phi) = \frac{1}{\tau_L[\Delta\omega(\Omega,\Phi)]^2} \qquad (4)$$

The frequency difference $\Delta\omega(\Omega,\Phi)$ for a probe at orientation Ω can be conveniently calculated from the directional derivative:[37] details of the calculation are given in the Appendix. For a small libration angle φ, it is found that $\Delta\omega \propto \varphi$, and therefore, the phase memory time depends on the product $\tau_L\varphi^2$.

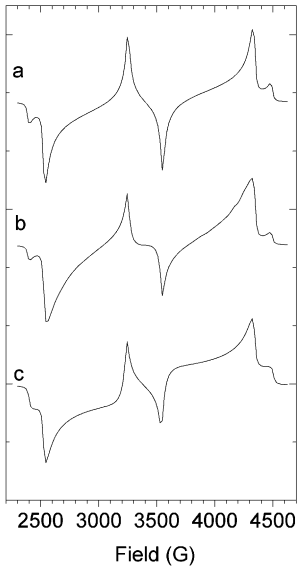

Figure 6. Calculated EchoEPR spectra at delay time $\tau = 160$ ns considering of a libration around the ZFS principal axes: (a) around the *X* axis, (b) *Y* axis, (c) *Z* axis. The simulations were obtained with the parameters given in Figure 3. For the decay of the magnetization we used $(1/T_M)^0_X = 600$ ns, $(1/T_M)^0_Y = 500$ ns, and $(1/T_M)^0_Z = 650$ ns and assumed a libration about the *Z* axis of the ZFS tensor with $\tau_L\varphi^2 = 0.8$ ps rad^2 (see text).

The calculated EchoEPR spectrum at time 2τ, as a function of the delay between the pulses, is obtained by multiplying each spin packet in eq 2 for the exponential $e^{-(2\tau)/(T_M(\Omega,\Phi))}$

$$I(B,2\tau) = \sum_{\pm}\int G(B_{res\pm}(\Omega) - B)P_{\pm}(\Omega)e^{-(2\tau)/(T_M(\Omega,\Phi))}\,d\Omega \quad (5)$$

It is worth considering in detail the differences, expected on the basis of this model, between the TR-EPR and the EchoEPR spectra by assuming a libration motion around each of the ZFS axes. The calculated spectra are reported in Figure 6.

For a libration around the *X* axis (Figure 6a), the EchoEPR spectrum shows a plateau with low intensity between the *X* and *Y* components, and a hole between the *Y* and *Z* components.

If the libration is around the *Y* axis (Figure 6b), the EchoEPR spectrum shows again a plateau with low intensity between the *X* and *Y* components, but with a milder slope in the vicinity of the *Y* components, and a hole between the *Y* and *Z* components.

For a libration around the *Z* axis (Figure 6c), shoulders appear in the vicinity of the *X* components, and no distortion of the line shape between the *Y* and *Z* components.

The comparison between the simulated and the experimental spectra indicates for the glassy toluene matrix (Figure 4) a libration around an axis close to the *Z* axis, whereas for the TPP matrix (Figure 5) a libration around an axis close to *Y*.

The ZFS axes are near to the inertial axes of the molecule. In particular, the *Y* axis is tilted by 15° with respect to the axis of the maximum elongation, and the *Z* axis is perpendicular to the molecular plane.[38] Therefore, the best agreement between experimental and simulated spectra for the TPP matrix corresponds to a libration of the DT molecule around the long molecular axis, parallel to the host channel axis, as expected in this constrained environment.

In the case of the toluene matrix the agreement between experimental spectra and simulations obtained for a libration around the *Z* axis is not as good as that in the previous case, suggesting a more complex motion, quite probable in this less hindering matrix. In a probable composite motion, the libration around the *Z* axis (perpendicular to the molecular plane) should represent the largest component.

A better understanding of the dynamical behavior in the two matrixes can be obtained by studying the EchoEPR profile as a function of the separation τ between the two echo-forming pulses.

For the toluene matrix, considering a libration around the *Z* axis, we have been able to reproduce the main features of the experimental spectra corresponding to τ delays of 160 and 200 ns, in particular the plateau between the *X* and the *Y* components. It has not been possible to obtain the deep between the *Y* and *Z* components, which is obtained only for rotations around the *X* or *Y* directions. This is a further indication that in toluene matrix the motion should be complex, with contributions from librations around different axes. In the simulations we have used a value $\tau_L\varphi^2 = 1.7$ ps rad^2. This type of motion is expected to produce a faster relaxation with respect to an uniaxial motion.

For the TPP matrix, we have considered the experimental spectra corresponding to τ delays of 160 and 320 ns the longer τ delay due to the slower relaxation in the TPP matrix with respect to toluene. The experimental line shape of the *Y* components, becoming sharper with increasing τ, is reproduced only by assuming a librational axis slightly tilted with respect to the *Y* ZFS principal direction. This result is in agreement with the expected rotation, which in the TPP matrix should be around the long molecular axis. The simulations have been obtained with a value $\tau_L\varphi^2 = 5.0$ ps rad^2.

The $\tau_L\varphi^2$ values used in the simulations have been tested by reproducing the experimental Hahn echo decay obtained in the two matrixes at 80 K for the low-field *Y* component. In our model, the individual values of the libration correlation time τ_L and of the motion amplitude φ cannot be disentangled. Because the ZFS values do not change in the range 4−80 K, φ has to be of the order of few degrees. By assuming $\varphi \simeq 0.1$ rad (6°), $\tau_L \simeq 500$ ps, in agreement with the typical libration correlation times measured in solids.[39]

Conclusions

The differences of the spectral profiles between time-resolved cw EPR spectra and EchoEPR spectra of photoexcited triplets of dithiophene in two solid matrixes have given detailed information on the motions of the excited molecule. The spectral profiles at 80 K have been satisfactorily simulated by considering the time modulation of the ZFS as the main echo dephasing cause. Similar effects have been already observed for a free-base porphycene triplet[29] and can be foreseen in any photoexcited triplet with ZFS parameters of similar magnitude.

The motions of the probe in the two matrixes, dissolved in glassy toluene and included in TPP, are found to occur around libration axes different for the two matrixes.

In the first case, the motion is found to be largely anisotropic, preferentially taking place around the axis perpendicular to the molecular plane of the aromatic rings. However, the simulations show that this model is a simplified one, and a more complex motion should be modeled, taking into account other degrees of freedom of the probe.

On the other hand, in the TPP matrix good fitting simulations are obtained with the model of an anisotropic librational motion exclusively around the axis of maximum elongation of the probe, parallel to the axis of the host channel. This conclusion is in agreement with solid-state NMR results described for several elongated molecules in confining matrixes of TPP and perihydrotriphenylene. In particular $^{13}C(T_1)$ relaxation times and

^{2}H NMR provided evidences for fast motion about the main axis of the molecule in the channels. The motion is still present at low temperature.[24,39−43]

Another piece of information can be anticipated to be in agreement with this model. Taking advantage of the higher melting temperature of the inclusion compound with respect to the toluene matrix we studied the TR-EPR spectra in TPP up to 240 K, as it will be reported in a paper in preparation.[38] The experimental spectra at this temperature show an averaging of the *X* and *Z* features, whereas the splitting between the *Y* features is unaffected, as expected if *Y* is the preferred reorientation axis.

The different dynamical behavior of the probe in the two solid matrixes gives also rise to different absolute rates of the echo dephasing, faster in toluene than in TPP, in agreement with the larger number of degrees of freedom for the librational motion in the latter matrix.

Appendix

The energies of the triplet states have been obtained by several authors by using the perturbation theory up to the second order (see references in ref 36). Moreover, they have been obtained also by exact calculation.[44] However, to obtain the variation of the resonance frequency for a reorientation of the probe it is convenient to obtain the energies as function of the Euler angles. We write, therefore, the fine interaction term in the spin Hamiltonian eq 1 with the spherical tensor notation:

$$\mathbf{S}\cdot\mathbf{D}\cdot\mathbf{S} = \sum_n T_{\mathbf{B}}^{(2,n)*} S^{(2,n)} \qquad \text{(A.1)}$$

where $S^{(2,n)}$ and $T_{\mathbf{B}}^{(2,n)}$ are the components for the spin operators and the interaction tensor, respectively, expressed in the laboratory frame defined by the magnetic field **B**. The values of the transition fields $B_{\pm}$, corrected up to the second order in the ZFS perturbation, may be obtained from the resonance condition:

$$\hbar\omega_0 = \mu_{\mathbf{B}} g B_{\mathrm{res}\pm} \pm \sqrt{(3/2)}T_{\mathbf{B}}^{(2,0)} + (2\mu_{\mathbf{B}} g B_{\mathrm{res}\pm})^{-1}\{|T_{\mathbf{B}}^{(2,1)}|^2 + |T_{\mathbf{B}}^{(2,2)}|^2\} \qquad \text{(A.2)}$$

Equation A.2 may be written explicitly in terms of the ZFS parameters *D* and *E* by transforming the tensor components to the principal axes frame:

$$T_{\mathbf{B}}^{(2,n)} = \sum_m D_{nm}^2(\alpha\beta\gamma) T_{\mathrm{ZFS}}^{(2,m)} \qquad \text{(A.3)}$$

where D_{nm}^2 are the Wigner rotation matrix elements.[45] The result reads as

$$\begin{aligned}\hbar\omega_0 = {} & \mu_{\mathbf{B}} g B_{\mathrm{res}\pm} \pm (1/2)\{D(3\cos^2\beta - 1) + 3E\sin^2\beta\cos 2\gamma\} + \\ & (16\mu_{\mathbf{B}} g B_{\mathrm{res}\pm})^{-1}\{2D^2\sin^2\beta(1 + 3\cos^2\beta) + \\ & 4DE(\sin^2\beta)(1 - 3\cos^2\beta)\cos 2\gamma + \\ & E^2(5 + 6\cos^2\beta - 3\cos^4\beta - 3\sin^4\beta\cos 4\gamma)\}\end{aligned} \qquad \text{(A.4)}$$

A rotation of the molecule around a given axis can be described by a reorientation of the magnetic field director $\mathbf{b}(\Omega)$ from position Ω_{in} to Ω_{fin} defined by the vector $\Phi = \mathbf{b}(_{\mathrm{fin}}) - \mathbf{b}(_{\mathrm{in}})$. For a small-angle motion, $\Phi \approx \varphi$ and the reorientation induces a resonance frequency change $\Delta\omega(\Omega,\Phi) \approx \nabla\omega(\Omega)\cdot\Phi \approx |\nabla\omega(\Omega)|\varphi\cos\xi$, where ξ is the angle between the gradient vector at fixed field and the displacement vector, and $\nabla\omega(\Omega)$ the gradient that can be calculated easily from eq A.4: if under a first-order approximation only the first two terms in eq A.4 are retained, then

$$|\nabla\omega(\Omega)| \propto |\nabla B_{\mathrm{res}\pm}| = \sqrt{\left(\frac{1}{\sin\beta}\cdot\frac{\partial B_{\mathrm{res}\pm}}{\partial\gamma}\right)^2 + \left(\frac{\partial B_{\mathrm{res}\pm}}{\partial\beta}\right)^2} \qquad \text{(A.5)}$$

References and Notes

(1) Langley, P. J.; J. Hulliger, J. *Chem. Soc. Rev.* **1999**, *28*, 279.
(2) Rodenberger, D. C.; Heflin, J. R.; Garito, A. F. *Nature* **1992**, *359*, 309.
(3) Lednev, I. K.; Ye, T.-Q.; Hester, R. E.; Moore, J. N. *J. Phys. Chem.* **1996**, *100*, 13338.
(4) Lochbrunner, S.; Fuss, W.; Schmid, W. E.; Kompa, K.-L. *J. Phys. Chem. A* **1998**, *102*, 9334.
(5) Hilinski, E. F.; McGowan, W. M.; Sears, D. F., Jr.; Saltiel, J. *J. Phys. Chem.* **1996**, *100*, 3308.
(6) del Valle, J. C.; Tarkalanov, N.; Saltiel, J. *J. Phys. Chem. B* **1999**, *103*, 9350.
(7) Bongiovanni, G.; Botta, C.; Brédas, J. L.; Cornil, J.; Ferro, D. R.; Mura, A.; Piaggi, A.; Tubino, R. *Chem. Phys. Lett.* **1997**, *278*, 146.
(8) Ohta, K.; Naitoh, Y.; Tominaga, K.; Hirota, N.; Yoshihara, K. *J. Phys. Chem. A* **1998**, *102*, 35.
(9) Anderson, N. A.; Pullen, S. H..; Walker, L. A.; Shiang, J. J.; Sension R. J. *J. Phys. Chem. A* **1998**, *102*, 10588.
(10) Bunker, C. E.; Lytle, C. A.; Rollins, V.; Sun, Y.-P. *J. Phys. Chem. A* **1997**, *101*, 3214.
(11) Biswas, N.; Umapathy, S. *J. Phys. Chem. A* **1997**, *101*, 5555.
(12) Ramamurthy, V.; Caspar, J. V.; Eaton, D. F.; Kuo, E. W.; Corbin, D. R. *J. Am. Chem. Soc.* **1992**, *114*, 3882.
(13) Ramamurthy, V.; Eaton, D. F. *Chem. Mater.* **1994**, *6*, 1128.
(14) Evans, C. H.; De Feyter, S.; Viaene, L.; van Stam, J.; De Schryver, F. C. *J. Phys. Chem.* **1996**, *100*, 2129.
(15) Caspar, J. V.; Ramamurthy, V.; Corbin, D. R. *J. Am. Chem. Soc.* **1991**, *113*, 600.
(16) Hoss, R., Koenig, O.; Kramer-Hoss, V.; Berger, U.; Rogin, P.; Hulliger, J. *Angew. Chem., Int. Ed. Engl.* **1996**, *35*, 1664.
(17) Hertzsch, T.; Kluge, S.; Weber, E.; Budde, F.; Hulliger, J. *Adv. Mater.* **2001**, *13*, 1864.
(18) Abou-Hamdan, A.; Bugnon, P.; Saudan, C.; Lye, P. G.; Merbach, A. E. *J. Am. Chem. Soc.* **2000**, *122*, 592.
(19) Li, G.; McGown, L. B. *Science* **1994**, *264*, 249.
(20) Pistolis, G.; A. Malliaris, A. *J. Phys. Chem.* **1996**, *100*, 15562.
(21) Sozzani, P.; Comotti, A.; Simonutti, R.; Meersmann, T.; Logan, J. W.; Pines, A. *Angew. Chem., Int. Ed.* **2000**, *39*, 2695.
(22) Meersmann, T.; Logan, J. W.; Simonutti, R.; Caldarelli, S.; Comotti, A.; Sozzani, P.; Kaiser, L. G.; Pines, A. *J. Phys. Chem. A* **2000**, *104*, 11665.
(23) Sozzani, P.; Comotti, A.; Simonutti, R.; Bracco, S.; Simonelli, A. In *Strength from motion in Crystals: The Example of Supramolecular Adducts*; Hargittai, I., Domenicano, A., Eds; NATO Science Series; Kluwer Academic Publishers: Dordrecht, 2002.
(24) Comotti, A.; Simonutti, R.; Catel, G.; Sozzani, P. *Chem. Mater.* **1999**, *11*, 1476.
(25) Atherton, N. M. *Principles of ESR*; Ellis Horwood and Prentice Hall: London, 1993.
(26) Dzuba, S. A. *Spectrochim. Acta A* **2000**, *56*, 227 and references therein.
(27) Husted, R.; Du, J. L.; Eaton, G. R.; Eaton S. S. *Magn. Reson. Chem.* **1995**, *33*, S66.
(28) Rohrer, M.; Gast, P.; Moebius, K.; Prisner T. F. *Chem. Phys. Lett.* **1996**, *259*, 523.
(29) Kay, C. W. M.; Elger, G.; Moebius K. *Phys. Chem. Chem. Phys.* **1999**, *1*, 3999.
(30) Comotti, A.; Simonutti, R.; Stramare, S.; Sozzani, P. *Nanotechnology* **1999**, *10*, 70.
(31) Zotti, G.; Gallazzi, M. C.; Zerbi, G.; Meille, S. V. *Synth. Met.* **1995**, *73*, 217.
(32) Bennati, M.; Grupp, A.; Mehring, M.; Baeuerle, P. *J. Phys. Chem.* **1996**, *100*, 2849.
(33) Segre, U.; Pasimeni, L.; Ruzzi, M. *Spectrochim. Acta A* **2000**, *56*, 265.
(34) Romanelli, M.; Kevan, L. *Concepts Magn. Reson.* **1997**, *9*, 403; *Concepts Magn. Reson.* **1998**, *10*, 1.
(35) Salikhov, K. M.; Tsvetkov, Yu. D. Electron Spin−Echo Studies of Spin−Spin Interactions in Solids. In *Time Domain Electron Spin Resonance*; Kevan, L., Schwartz, R. N., Eds.; Wiley-Interscience: New York, 1979; pp 231−277.

(36) Weil, J. A.; Bolton, J. R.; Wertz, J. E. *Electron Paramagnetic Resonance. Elementary Theroy and Practical Applications*; J. Wiley & Sons: New York, 1994.

(37) Thomas, G. B.; Finney, R. L. *Calculus and Analytical Geometry*; Addison-Wesley Publishing Co.: Reading, MA, 1979.

(38) Barbon, A.; Bortolus, M.; Brustolon, M.; Comotti, A.; Maniero, A. L.; Sozzani, P. **2003**. In preparation.

(39) Dzuba, S. A. *Phys. Lett. A* **1996**, *213*, 77.

(40) Sozzani, P.; Behling, R. W.; Schilling, F. C.; Bruckner, S.; Helfand, E.; Bovey, F. A.; Jelinski, L. W. *Macromolecules* **1989**, *22*, 3318.

(41) Sozzani, P.; Amundson, K. R.; Schilling, F. C. *Macromolecules* **1994**, *27*, 6498.

(42) Sozzani, P.; Simonutti, R.; Comotti, A. *Mol. Cryst. Liq. Cryst.* **1996**, *277*, 299.

(43) Sozzani, P.; Bovey, F. A.; Schilling, F. C. *Macromolecules* **1989**, *22*, 4225.

(44) Anderson, R. J. M.; Kohler, B. E. *J. Chem. Phys*. **1975**, *63*, 5081.

(45) Brink, D. M.; Satchler, G. R. *Angular Momentum*; Oxford University Press: Oxford, 1968.